ACS OMEGA

http://pubs.acs.org/journal/acsodf

Article

NaCl Crystals as Carriers for Micronutrient Delivery

Simon E. G. Lepinay, Raymond Nijveld, Krassimir P. Velikov,* and Noushine Shahidzadeh*

Cite This: *ACS Omega* 2022, 7, 28955−28961

Read Online

ACCESS | Metrics & More | Article Recommendations

ABSTRACT: Iron deficiency leading to anemia is one of the most severe and important nutritional deficiencies in the world today. To combat this deficiency, the fortification of food products with iron is a natural way to increase the global iron uptake. Here, we report a novel strategy for iron encapsulation in NaCl crystals via microscopic inclusions containing dissolved iron salt. The liquid inclusions embedded in the crystal insulate the reactive iron salts from their environment while assuring that iron is in a soluble and bioavailable form. While the size distribution of inclusions remains independent of the evaporation conditions, their density increases during crystallization at lower relative humidity. Using Raman confocal microspectroscopy, we have been able to analyze the morphology, length/thickness ratio, of inclusions and show that inclusions evolve toward a plate-like structure with the increase in size. By growing a pure NaCl shell around the iron-containing NaCl crystals, the stability of the composite crystals can be even further enhanced. The role of halite crystals as a carrier for iron fortification opens the way for the delivery of other types of micronutrients by including them in table salt.

1. INTRODUCTION

Crystallization processes are widely used for the manufacturing of food products, fine chemicals, and pharmaceuticals. Generally, in order to obtain products with desired solid-state properties and a reproducible crystal size, habit, and form, purification or controlling impurity incorporation remains an important step as they act both on the thermodynamics and on the kinetics of crystallization. For this reason, recent works have focused on both purification[1,2] and on trying novel approaches for the prevention of impurity incorporation. However, a complete understanding of impurity rejection or incorporation mechanisms is still elusive, even though it may greatly help to control crystal size distributions and polymorph control.

In this paper, we focus on the incorporation of a very specific "impurity" in common table salt. We use the incorporation of impurities to our advantage: we aim to deliver iron in a bioavailable and stable form by adding it to table salt. The approach is inspired by the naturally occurring Himalayan salt. Himalayan salt naturally incorporates traces of various minerals[3,4] giving its characteristic pink hue. However, the presence of heavy metals and the low Fe/Na ratio (5−220)[3,4] limit its use as an iron delivery system. Iron deficiency-related anemia remains one of the most severe and important nutritional deficiencies in the world today.[5] Iron deficiency impairs the cognitive development of children from infancy through to adolescence. It damages immune mechanisms and is associated with increased morbidity rates. Much as has been done for iodine in the past, iron fortification of food products appears to be a natural avenue to pursue. This indeed has already been attempted in several systems (e.g., bouillon cubes, soy sauces, wheat flour, and table salt) by including pure or encapsulated iron salts.[5,6] The main challenge there is that the presence of iron can cause adverse reactions such as hydrolysis, complexation of phytochemicals, and lipid oxidation, which can cause metallic taste, rancidity, or color changes.[6] In addition, when designing an iron fortification strategy, choosing an iron compound with increased storage stability means decreasing reactivity. This is often achieved either by encapsulating or tuning the solubility of the iron compound.[5] Encapsulation is generally regarded as expensive, and the use of iron compounds with lower water solubility generally makes the iron less bioavailable.[7,8] To address this problem, microencapsulation at low cost has been explored to some extent.[7,8]

Table salt, sodium chloride, is a very attractive vehicle for iron delivery due to its widespread use in our diet. However, incorporation of iron as already discussed faces several challenges associated with color change and homogeneous distribution throughout the salt crystals (because of the differences in grain size, shape, and density between NaCl and the iron salts).[5,9,10] Here, we report on novel NaCl crystalline materials fortified with iron using primary liquid inclusion strategy as the incorporation mechanism where pockets of mother liquor containing the micronutrient can be entrapped during growth.

Most of the studies on fluid inclusions in halite are mainly oriented on their composition and their implications in geology as time capsules,[11] on the history of seawater and the survival of

Received: April 25, 2022
Accepted: July 1, 2022
Published: August 10, 2022

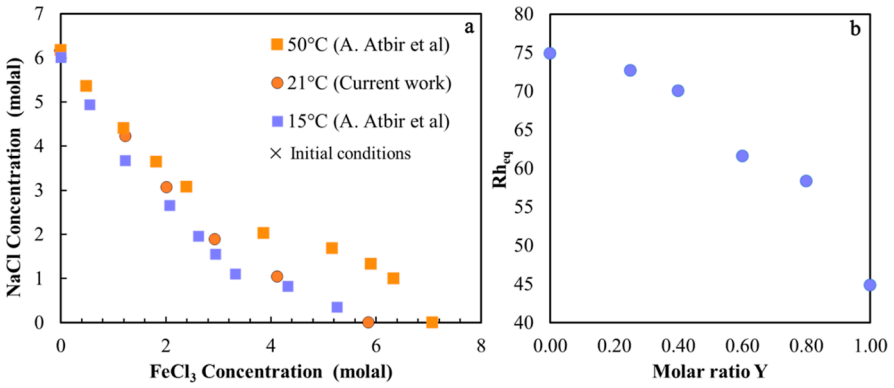

Figure 1. (a) Solubility curve of the ternary NaCl−$FeCl_3$−H_2O system and the initial composition points (italics: $Y = \frac{n_{Fe}}{n_{Fe} + n_{Na}}$) for crystallization by evaporation experiments. (b) Equilibrium RH (RH_{eq}) above the saturated salt solution at different Y ratios at 21 °C.

microorganisms.[12] Little is known about the kinetics of liquid inclusion formation, their size distribution, and form with respect to the initial conditions of the NaCl growth. Generally, when fluid inclusions are trapped during the growth of the crystal, we talk about primary fluid inclusions, whereas secondary inclusions consist of liquid trapped along fractures that develop and heal long after the crystal has formed.

Here, we present a quantitative analysis of the number and size distribution of the microliquid inclusions embedded in the crystals during the solution crystallization process by tuning the evaporation rate and the stirring. In addition, we have been able to define the relation between the size and the morphology of the microinclusions and the amount of incorporated iron using Raman confocal microscopy and inductively coupled plasma−optical emission spectrometry (ICP−OES). The table salt consequently plays the role of a carrier for the delivery of iron (at the desired concentration fitting the daily authorized amount[13]) in a water-soluble, bioavailable form. Finally, we describe how to increase the stability of the novel iron fortified salt even further based on core−shell growth of a pure sodium chloride layer.

2. EXPERIMENTAL SECTION

2.1. Salt Mixture Solution Preparation. Mixed solutions of NaCl (BioXtra, >99.5%) and $FeCl_3 \cdot 6H_2O$ (Sigma-Aldrich grade, >99%) slightly below saturation were prepared for bulk evaporation experiments. For this purpose, the solubility curve of the mixed salt was determined. This was done by progressively adding solvent to the salt mixtures until complete dissolution. The solutions were prepared at 21 ± 1 °C by weighing a constant mass of NaCl (10 g) and adding the corresponding mass of $FeCl_3 \cdot 6H_2O$ and 0.1 M HCl in Millipore water (18.2 MΩ·cm) defined as the solvent in this work to fit the iron-to-sodium molar ratio Y.

$$Y = \frac{n_{Fe}}{n_{Fe} + n_{Na}} \quad (1)$$

where n_i is the quantity of element i in moles.

Experiments were performed at three Y ratios: 0.1, 0.25, and 0.4. The HCl solution is needed to maintain the pH under 2 and inhibit the hydrolysis of Fe(III).[14]

2.2. Solubility Determination. The solubility points for each molar ratio Y were established by subsequent additions of the solvent by increments of 100 μL. At each step, the suspensions were stirred for 6 h. The solubility point is defined when a transparent homogeneous salt solution is obtained.

2.3. Crystallization by Evaporation. Bulk evaporation experiments have been performed, at each molar ratio Y, with mixed-salt solutions at saturation $\beta = \frac{m^i_{NaCl}}{m^s_{NaCl}} \sim 0.95$ (where $m_{NaCl}{}^i$ is the weighed mass and $m_{NaCl}{}^s$ is the mass of sodium chloride at saturation) to avoid the presence of any crystalline seeds. The evaporation experiments are carried out at relative humidity (RH) = 20 ± 2.5% and RH = 60 ± 2.5% corresponding to a fast and slow evaporation rate, respectively. The RH in the chamber was regulated to the desired RH thanks to a homemade automated feedback-controlled nitrogen flow system.

In addition, the impact of stirring (0 and 60 rpm) during evaporation on crystal precipitation has also been investigated at each RH. The evaporation experiments were stopped before the crystals broke the surface, as this would cause solution pooling and eventually staining. The precipitated crystals were subsequently removed and rinsed with ethanol (purity 99.8%) and analyzed carefully using Raman confocal microspectroscopy, scanning electron microscopy (SEM), and ICP−OES. The washing step is aimed to eliminate all traces of $FeCl_3$ at the surface of crystals that could further hydrolyze when aging in ambient conditions.

2.4. Scanning Electron Microscopy. A tabletop TM3000 Hitachi scanning electron microscope was used with an accelerating voltage of 15 kV to measure the size distribution of the salt crystals and morphology information. ImageJ was then used to automate grain detection and estimate their size.

2.5. Elemental Composition Analysis by ICP−OES. The elemental composition of the crystals was analyzed with ICP−OES. This technique inductively heats microdroplets (mist) of the analyte solution until a plasma is formed. The characteristic spectrum of this plasma is used against a reference to determine the initial elemental composition. In our experiments, the collected crystals from bulk crystallization of the mixed salt solution were ground and dissolved using a nitric acid solution (70%, purified by redistillation, ≥99.999% trace metals, Sigma-Aldrich). The solutions were then analyzed on duplicates with ICP−OES (Agilent 5110 VDV in the dual mode) using scandium as an internal standard.

2.6. Raman Confocal Microspectroscopy. Raman confocal microspectroscopy was performed using a WITec, Alpha 300 R microscope coupled to a CMOS camera (Andor, Newton EMCCD, DU970P-BVF-355). The laser wavelength used was 532 nm with a diffraction grating of 600 g·mm^{-1}. While Raman spectra provide an extensive chemical, physical, and structural insight into a local point of interest in the sample,

https://doi.org/10.1021/acsomega.2c02572
ACS Omega 2022, 7, 28955−28961

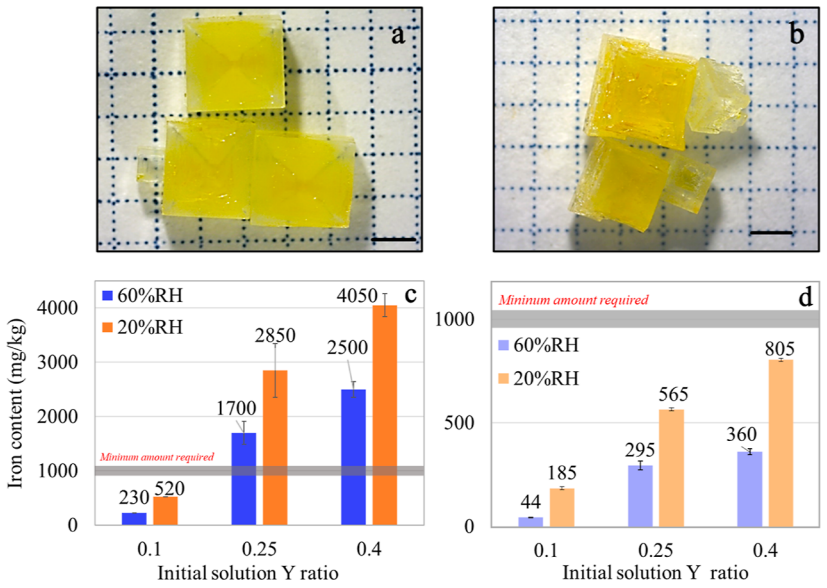

Figure 2. Crystals obtained at iron molar ratio $Y = 0.25$ and RH: (a) RH = 60 ± 5% and (b) RH = 20 ± 5%. Scale bar is 1 mm. (c) ICP−OES measurement of iron content in crystals formed at different relative humidities and different molar ratios Y and (d) iron content of the same crystals after grinding and washing.

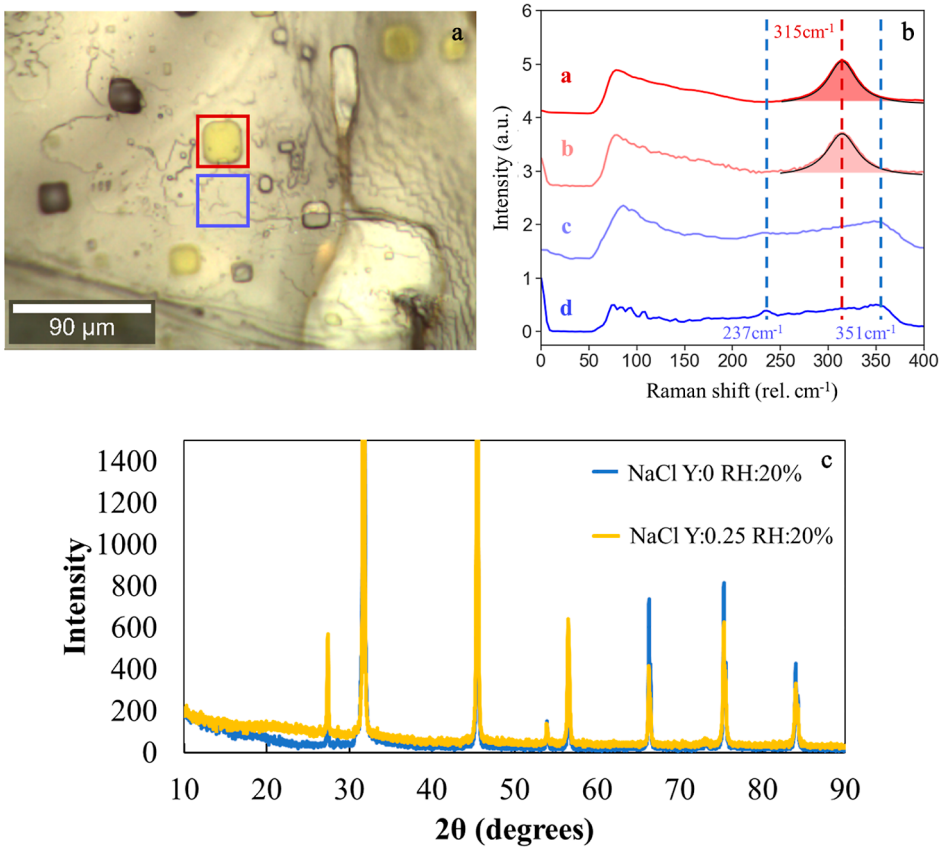

Figure 3. (a) Microscopy picture of a crystal and its inclusions ($Y = 0.25$, RH = 20%). (b) Raman spectra comparison: (a) reference NaCl/$FeCl_3$ solution $Y = 0.5$ and $C_{NaCl} = 3$ M, (b) inclusion spectrum, (c) crystal spectrum, and (d) reference NaCl crystal. Dotted lines are guide for the eyes indicating peaks. (c) X-ray powder diffractogram comparison between pure NaCl (blue) and a representative sample of fortified salt (yellow).

confocal microscopy enables high-resolution volume analysis within the sample in both the lateral (XY) and axial (Z) axes. Thus, the technique brings high-resolution chemical imaging of the precipitated crystals at the microscale.

2.7. Stability over Time. The stability of the precipitated crystals containing iron has been investigated by means of color change due to the oxidation of iron over time. For the latter, the crystals were stored at 40 ± 1 °C and RH = 30 ± 2.5% up to 18

https://doi.org/10.1021/acsomega.2c02572
ACS Omega 2022, 7, 28955−28961

months. Images have been taken regularly to follow the color and surface aspect of the crystals.

3. RESULTS AND DISCUSSION

As can be observed in Figure 1, addition of one salt decreases the solubility of the other: the higher the proportion of iron in the mixture, the lower is the solubility of NaCl. Our results at room temperature agree well with those obtained at 15 and 50 °C.[15] In addition, as the concentration of the iron in the solution increases, the water vapor pressure (above the resulting solution) is also lowered (Figure 1). With drying and water evaporation, the mixed salt solution reaches its solubility limit, and subsequently nucleation in the solution can be observed. The precipitated crystals have a cubic morphology similar to sodium chloride with a yellow hue.

We show in Figure 2a,b that the fast evaporation rate (RH = 20%) leads to a more heterogeneous crystal size with more defects in their morphology. In Figure 2c, using ICP−OES analysis, the concentration of iron content in crystals is determined and plotted against the initial iron molar ratio Y for the two evaporation conditions. The results clearly show that iron is present in the NaCl crystals, which can explain the yellow color of the crystals. For a given Y, the amount of embedded iron is higher than the minimum daily amount required (850−1100 mg·kg^{-1} by the FSSAI)[13] showing that the desirable range of embedded iron can be achieved. The faster evaporation rate at RH = 20% increases the iron content by a factor > 1.6 compared to crystallization at RH = 60% because of a higher inclusion density as is further evidenced through this paper. Moreover, as illustrated by the pictures from Figure 2, this increase is not reflected by a change in morphology or color.

Several potential mechanisms can explain how iron is incorporated in sodium chloride crystals: (a) the existence of a double salt, (b) the formation of fluid inclusions, and (c) the existence of a solid solution domain. The latter corresponds to a solid-state compound of formula $A_{1-x}B$ where the pure compound B is accepted in A's structure via defects (substitutional or interstitial). Generally, the charge and radius differences between Na^+ and Fe^{3+} ions are believed to limit the extent to which Fe^{3+} ions can be present in the crystalline structure as defects.[16] However, it has been shown that yttrium ion Y^{3+} doping of NaCl is possible up to 118 via melt crystallization.[16] The absence of new peaks or peak shifts on the XRPD diffractogram (Figure 3) leads us to dismiss the double salt hypothesis. Consequently, to demonstrate whether we have fluid inclusions[17,18] or a solid solution, the crystals were ground to powder and washed with ethanol. The ICP analysis of the resulting powder show that there is a reduction of at least 80% of iron content for a given ratio, which strongly suggests that the dominant mechanism for iron incorporation is the formation of pockets of solution (liquid inclusions) during crystal growth, which has been then removed during the washing step with ethanol. The remaining quantified iron content could be further explained by a group of still intact inclusions in the ground crystals, as the shift in the X-ray diffraction pattern characteristic of solid solution is absent in the ground powder (Figure 3).

The composite crystals were also analyzed at the microscale using Raman confocal and optical microscopy techniques. The imaging of the crystalline facets under the microscope confirms the presence of microscale yellow pockets (Figure 3). The Raman spectra of these regions reveals a peak at 315 cm^{-1} characteristic of the cation complex $FeCl_3$,[19] which is also present for the solution of $FeCl_3$ as well as a shifted OH stretching band at ∼3500 cm^{-1}. These results confirm that primary liquid inclusion is the mechanism by which iron is entrapped in the crystalline structure during the growth.

2D Raman microspectroscopy mapping in the XY and XZ plane was performed to get information on the geometry of the liquid inclusions. The intensity resulting from the integration of the $FeCl_3$ Raman peak (315 ± 50 cm^{-1}) on an inclusion is shown in Figure 4b. The analysis of various inclusions shows that

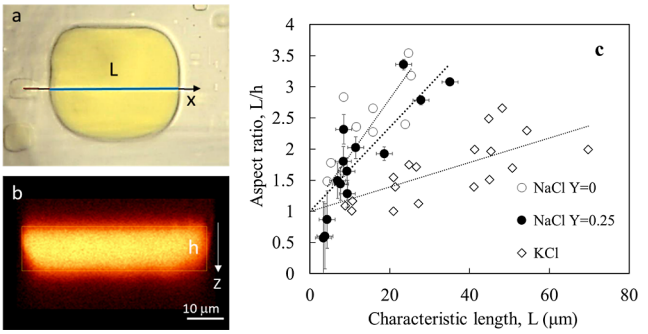

Figure 4. Confocal Raman spectromicroscopy of inclusions: (a) XY position of the 2D scan of an inclusion and (b) XZ Raman mapping intensity. Brighter yellow corresponds to higher iron content; (c) aspect ratio (L/h) of inclusions plotted against their characteristic length L for NaCl crystals precipitated from pure NaCl solution, from solution with Y = 0.25 of Fe, and for KCl crystals extracted from Cline et al.[20]

the aspect ratio varies with the size of the inclusion (Figure 4c). Therefore, the inclusions are not systematically cube like as it is reported in the literature.[19,20] In these previous works, the liquid inclusions were observed using 2D optical microscopy and consequently were assumed to be cubic as monitoring the depth of the inclusions was not possible.[21,22] The change in the aspect ratio as a function of inclusion diameter has also been reported in an earlier work on KCl crystals by Cline and Anthony[20] (by making photography at 2 different angles). In Figure 4, their results are compared to ours for the case of NaCl crystals precipitated from pure NaCl solution and from the solution at Y = 0.25 by using confocal Raman microscopy. Thanks to this highly advanced technique, we were able to precisely measure the thickness of the inclusions as it allows for accurate depth imaging resulting in higher sensitivity to the 3D structure. Our results confirm well the fact that primary inclusions evolve toward a plate-like structure at larger size.

The growth rate of a crystal is the result of the superposition of surfaces, layer by layer. These layers are formed by growth units that can be integrated at the surface of the crystal. For a crystal surface to grow in its supersaturated solution, ions have to be transported by diffusion and convection from the bulk before they can be incorporated into the crystal structure. If the crystal growth is controlled by diffusion, the concentration in solution surrounding the faces and edges of the growing crystal would have a non-uniform distribution of concentration, which will lead to a preferential growth as two-dimensional nucleation forming moving steps. The differential growth rates can subsequently induce the formation of fluid (mother liquid) inclusions on the imperfections of the surface of a crystal in bands parallel to halite crystal growth faces. This would subsequently favor a plate-like geometry for the imperfection.

We have also compared the liquid inclusions of our iron NaCl crystals with NaCl crystals obtained from pure NaCl solution in the same evaporation conditions. The composition of the

https://doi.org/10.1021/acsomega.2c02572
ACS Omega 2022, 7, 28955−28961

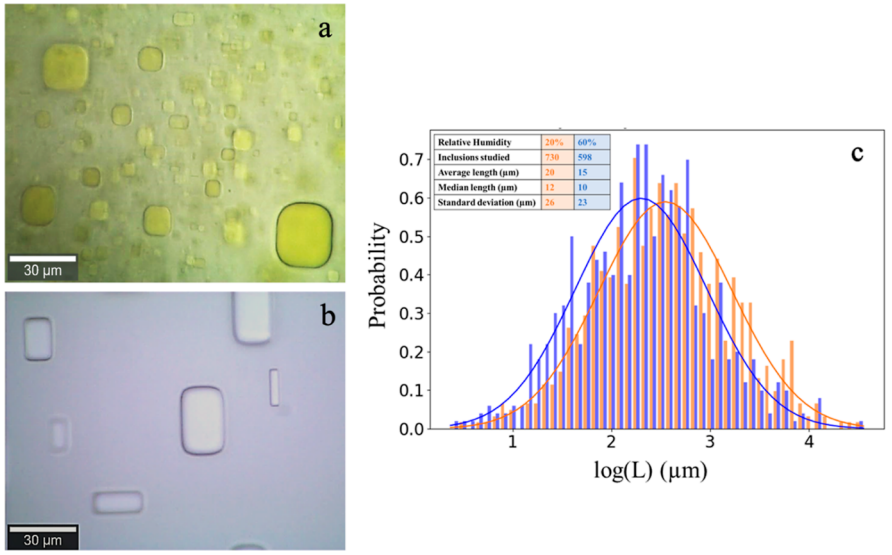

Figure 5. (a) Optical microscopy picture of a crystal's inclusions (Y = 0.25, RH = 20%). (a) Optical microscopy picture of a crystal's inclusions (Y = 0.25, RH = 20%). (b) Comparison with liquid inclusions in NaCl crystals precipitated in pure NaCl solution at RH ∼ 20%. (c) Inclusion size distribution comparison between precipitated crystals at different RHs for Y = 0.25; inset: table reporting the data measured.

solution (with a lot of Fe) plays an important role in the density of inclusions compared to those obtained from pure NaCl solution at the same evaporation rate. The existence of Fe as impurities in solution influences the growth mechanism; by adsorbing on the surface of the crystals, they can prevent the progression of the growth units on the surface, forcing the growing steps to pass between the impurities and increasing the number of liquid inclusions, as can be seen in Figure 5a,b.

The effect of RH on the size distribution of inclusions has been quantified by using ImageJ's contrast-enhancing techniques (Figure 5c). It is interesting to note that, although evaporation at low RH leads to an increase of the inclusion density by increasing the total volume of inclusions, the size distribution of the inclusions remains independent of evaporation conditions. The inclusion size distribution should be affected by the crystal size (smaller crystals would have fewer liquid inclusions). In our experiments, at low and high RH, the size of the crystals is almost equivalent.

The evaporation rates at RH = 20% and RH = 60% are around 4.1×10^{-5} and 3.2×10^{-6} cm^3/s, respectively. Faster evaporation rate of water can induce a non-uniform distribution of ions in the solution; the latter can be estimated by calculating the Peclet number Pe, which gives an indication of the rate of advection of ions by the flow to the rate of diffusion in the salt solution $Pe = LU/D$, where L is the characteristic length of displacement in the beaker, U is the speed of evaporation, and D is the diffusion coefficient of Na^+ in the saturated salt solution (0.68×10^{-5} cm^2/s).[23] The estimation of the Peclet number in our experimental conditions gives a $Pe \sim 0.9$ at RH 20% and $Pe \sim 0.07$ for RH 60%. Clearly at higher evaporation rates, because the rate of advection of ions to the evaporative surface is of the same range than the rate of diffusion, a more heterogeneous solution is created. This leads subsequently to a non-uniform solution promoting asymmetrical growth and imperfections in the precipitated crystals. The non-uniform distribution of concentration surrounding the faces and edges leads to crystal growth controlled by diffusion and to a preferential growth as two-dimensional nucleation forming moving steps. As growth rate is generally different for each face of crystal and at edges and corners, the differential growth rates can subsequently induce the entrapment of fluid (mother liquid) inclusions on the imperfections of surface of a crystal in bands parallel to halite crystal growth faces during precipitation. Environmental parameters such as wall effects and confinement in addition to the evaporation conditions can influence such asymmetrical face growth and the density of inclusion entrapment during the growth.

At high and low RH, the growth mechanism and liquid inclusion formation as defects in the crystalline faces remains the same in the presence of Fe impurities; subsequently, higher evaporation rate increases the number of inclusions while their morphology and size distribution remains the same.

In industrial processes, crystallization can involve stirring for homogeneity concerns; therefore, we have also investigated the effect of stirring on the iron content via inclusions on precipitated crystals at different evaporation conditions. As can be seen in Figure 6, the average size of precipitated crystals

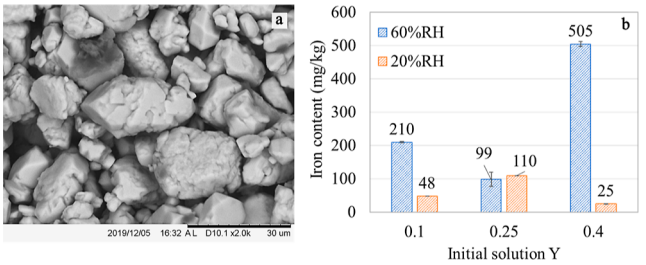

Figure 6. (a) SEM picture of the precipitated crystals while the solution was continuously stirred during evaporation and (b) iron content of NaCl crystals formed at 60 rpm stir rate for two evaporation conditions.

analyzed by SEM is found to be much smaller than crystallization without stirring; the average size is found to be 50 μm. Surprisingly, fast evaporation rate with stirring greatly reduces the amount of incorporated iron in the crystals contrary to what has been measured without stirring. In addition, higher molar ratio of iron Y does not lead systematically to higher iron content either; therefore, there is no direct correlation. There

https://doi.org/10.1021/acsomega.2c02572
ACS Omega 2022, 7, 28955−28961

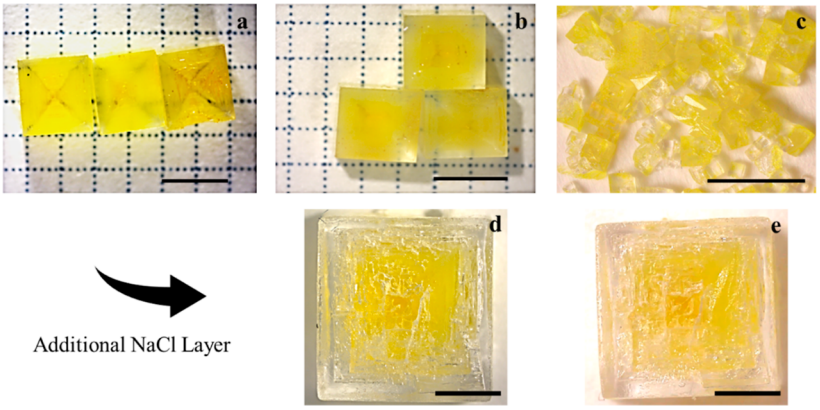

Figure 7. Stability of the crystals over time. Top: NaCl crystals with iron inclusions (fortified crystals); bottom: NaCl core−shell protected fortified crystals. Storage time: (a) initial state, (b,d) 1, and (c,e) 18 months. Scale bar 2 mm.

are two reasons which explain why stirring leads to much lower liquid inclusion density for the same evaporation condition. Stirring is known to increase the secondary nucleation,[24] leading to an overall smaller size of the crystals in a larger quantity. Previous work has shown that inclusions do not form in sodium chloride in the crystals that are smaller than 60 μm,[18] in line with the iron content reported in our microcrystals. In addition, generally an integration-controlled growth mechanism is needed in order to have a symmetrical growth of crystal surfaces and corners without imperfections. To achieve this, ion transport due to convection, for example, should remain faster than the ionic surface integration. One way to have these conditions and induce symmetrical growth is to keep crystals suspended in the solution by stirring or freely hanging in the solution.

Finally, to determine the stability over time of our novel crystalline materials, the latter were stored in an oven at 40 °C and RH = 30% up to 18 months. As shown in Figure 7, the yellow iron-containing NaCl crystals do not exhibit any signs of hydrolysis or discoloration over time. Nevertheless, a core−shell strategy was thought as a supplementary solution for a better protection and guarantee of the stability in larger scale experiments where some problems such as crystals breaking during handling or poor washing ability could decrease the stability. For this purpose, the crystals containing iron inclusions were immersed in a pure NaCl solution slightly below the saturation (0.95) and left to evaporate at high RH = 60% for 10 days. The yellow crystals act consequently as seeds for the further growth of pure sodium chloride during evaporation, and NaCl grows subsequently as a transparent shell at the outer surface of the yellow crystals making a protective layer. Such added layer of protection against breaks and leaks might be needed when scaling up the crystallization production (Figure 7).

CONCLUSIONS

In this paper, we have investigated how iron in a water-soluble form can be incorporated into NaCl crystals from a mixed NaCl and $FeCl_3$ solution to make iron-fortified table salts. We find that high loads (500−4000 mg·kg^{-1}) of iron can be incorporated in a controlled way in NaCl crystals by using its propensity to embed primary liquid inclusions during growth. The inclusion density can be controlled while keeping the size distribution constant by tuning the evaporation rate during the solution crystallization process: the inclusion density increases when crystallization occurs at low RH (high evaporation rate). We also show that liquid inclusions can be drastically reduced by stirring the solution as the latter leads to smaller crystals and promotes symmetrical growth due to convection. The inclusion morphology is found by confocal Raman microscopy to evolve toward a plate-like shape as their size increases. The iron-containing NaCl salt obtained in this way is shown to be stable up to 18 months in ambient conditions (RH = 60%/T = 20 °C). A core−shell strategy is shown to be a simple and efficient way to reinforce even more the stability of the products. Finally, as the formation of inclusions does not rely specifically on iron, their role as iron carriers described in this work could be generalized to the delivery of other types of micronutrients.

AUTHOR INFORMATION

Corresponding Authors

Krassimir P. Velikov − *Van der Waals-Zeeman Institute (WZI), Institute of Physics, University of Amsterdam, 1098 XH Amsterdam, Netherlands; Unilever Innovation Centre Wageningen, 6708 WH Wageningen, The Netherlands; Soft Condensed Matter, Debye Institute of Nanomaterials Science, Utrecht University, 3584 CC Utrecht, The Netherlands;* orcid.org/0000-0002-8838-1201; Email: krassimir.velikov@unilever.com

Noushine Shahidzadeh − *Van der Waals-Zeeman Institute (WZI), Institute of Physics, University of Amsterdam, 1098 XH Amsterdam, Netherlands;* orcid.org/0000-0003-2692-0764; Email: n.shahidzadeh@uva.nl

Authors

Simon E. G. Lepinay − *Van der Waals-Zeeman Institute (WZI), Institute of Physics, University of Amsterdam, 1098 XH Amsterdam, Netherlands;* orcid.org/0000-0003-3936-3741

Raymond Nijveld − *Nouryon Specialty Chemicals, 7418 AJ Deventer, The Netherlands*

Complete contact information is available at: https://pubs.acs.org/10.1021/acsomega.2c02572

Notes

The authors declare no competing financial interest.

ACKNOWLEDGMENTS

This work was performed in the public−private partnership "IRONTECH" and was financed by participating industrial partners Unilever Research and Development Wageningen B.V.,

https://doi.org/10.1021/acsomega.2c02572
ACS Omega 2022, 7, 28955−28961

Nouryon Chemicals B.V., Nobian B.V., and allowances of the Netherlands Organization for Scientific Research (NWO) in the framework of the Innovation Fund for Chemistry and from the Ministry of Economic Affairs in the framework of the "TKI/PPS-Toeslagregeling". Project number 731.017.205 of the research program TA which is (partly) financed by the Dutch Research Council (NWO).

REFERENCES

(1) Urwin, S. J.; Levilain, G.; Marziano, I.; Merritt, J. M.; Houson, I.; Ter Horst, J. H. A Structured Approach To Cope with Impurities during Industrial Crystallization Development. *Org. Process Res. Dev.* **2020**, *24*, 1443−1456.
(2) Capellades, G.; Bonsu, J. O.; Myerson, A. S. Impurity incorporation in solution crystallization: diagnosis, prevention, and control. *CrystEngComm* **2022**, *24*, 1989−2001.
(3) Barakat, A.; Maurice, S.; Roberts, C.; Benvenuto, M. A.; Roberts-Kirchhoff, E. S. Analysis of Salts and Salt Substitutes with a Handheld X-Ray Fluorescence Analyzer. *Trace Materials in Air, Soil, and Water*; ACS Symposium Series; American Chemical Society, 2015; pp 101−114.
(4) Yalçin, Ş.; Mutlu, İ. Structural Characterization of Some Table Salt Samples by XRD, ICP, FTIR and XRF Techniques. *Acta Phys. Pol., A* **2012**, *121*, 50−52.
(5) Pasricha, S.-R.; Tye-Din, J.; Muckenthaler, M. U.; Swinkels, D. W. Iron deficiency. *Lancet* **2021**, *397*, 233−248.
(6) Hurrell, R. F. Iron Fortification Practices and Implications for Iron Addition to Salt. *J. Nutr.* **2021**, *151*, 3S−14S.
(7) Shields, A.; Ansari, M. A. Review of Experience of the Production of Salt Fortified with Iron and Iodine. *J. Nutr.* **2021**, *151*, 29S−37S.
(8) Modupe, O.; Diosady, L. L. Quadruple fortification of salt for the delivery of iron, iodine, folic acid, and vitamin B12 to vulnerable populations. *J. Food Eng.* **2021**, *300*, 110525.
(9) Bijlsma, J.; de Bruijn, W. J. C.; Hageman, J. A.; Goos, P.; Velikov, K. P.; Vincken, J.-P. Revealing the main factors and two-way interactions contributing to food discolouration caused by iron-catechol complexation. *Sci. Rep.* **2020**, *10*, 8288.
(10) Blanco-Rojo, R.; Vaquero, M. P. Iron bioavailability from food fortification to precision nutrition. A review. *Innovative Food Sci. Emerging Technol.* **2019**, *51*, 126−138.
(11) Lazar, B.; Holland, H. D. The analysis of fluid inclusions in halite. *Geochim. Cosmochim. Acta* **1988**, *52*, 485−490.
(12) Toboła, T. Raman spectroscopy of organic, solid and fluid inclusions in the Oldest Halite of LGOM area (SW Poland). *Spectrochim. Acta, Part A* **2018**, *189*, 381−392.
(13) FSSAI. *Food Safety and Standards (Fortification of Foods) Regulations*; Gazette of India, 2018; Part III, Section 4.
(14) Flynn, C. M., Jr. Hydrolysis of inorganic iron(III) salts. *Chem. Rev.* **1984**, *84*, 31−41.
(15) Atbir, A.; Marrouche, A.; El Hadek, M.; Cohen-Adad, R.; Cohen-Adad, M. Équilibre solide-liquide du système quaternaire K+, Na+, Fe3+/Cl−H2O à 15 et 30 °C. *J. Chim. Phys.* **1997**, *94*, 1274−1285.
(16) Beniere, F.; Rokbani, R. Transport processes in NaCl single crystals doped with a trivalent cation; solubility, association, and migration of Y^{3+}. *J. Phys. Chem. Solids* **1975**, *36*, 1151−1160.
(17) Halasz, S.; Nakai, T. Specially Grown Salt Crystals for Carrying Additives. *7th Symposium on Salt*, 1993; Vol. *II*, pp 213−218.
(18) Saito, N.; Yokota, M.; Fujiwara, T.; Kubota, N. Liquid inclusions in crystals produced in suspension crystallization. *Chem. Eng. J.* **2000**, *79*, 53−59.
(19) Scholten, L.; Schmidt, C.; Lecumberri-Sanchez, P.; Newville, M.; Lanzirotti, A.; Sirbescu, M.-L. C.; Steele-MacInnis, M. Solubility and speciation of iron in hydrothermal fluids. *Geochim. Cosmochim. Acta* **2019**, *252*, 126−143.
(20) Cline, H. E.; Anthony, T. R. The shape relaxation of liquid droplets in solids. *Acta Metall.* **1971**, *19*, 175−180.
(21) Garmashov, S. I. A model of shapes of liquid cylindrical inclusions migrating through a non-uniformly heated crystal: Fundamentals and applications for studying crystallization and dissolution. *J. Cryst. Growth* **2021**, *574*, 126312.
(22) Davis, D. W.; Lowenstein, T. K.; Spencer, R. J. Melting behavior of fluid inclusions in laboratory-grown halite crystals in the systems NaCl;H2O, NaCl;KCl;H2O, NaCl;MgCl2;H2O, and NaCl;CaCl2;-H2O. *Geochim. Cosmochim. Acta* **1990**, *54*, 591−601.
(23) Shahidzadeh, N.; Schut, M. F. L.; Desarnaud, J.; Prat, M.; Bonn, D. Salt stains from evaporating droplets. *Sci. Rep.* **2015**, *5*, 10335.
(24) Ploß, R.; Mersmann, A. A new model of the effect of stirring intensity on the rate of secondary nucleation. *Chem. Eng. Technol.* **1989**, *12*, 137−146.

https://doi.org/10.1021/acsomega.2c02572
ACS Omega 2022, 7, 28955−28961